

Dark Matter Annihilation and the Dwarf Spheroidals

N.W. Evans ¹, F. Ferrer ² and S. Sarkar ²

¹ Institute of Astronomy, University of Cambridge, Madingley Road, Cambridge CB3 OHA, UK

² Theoretical Physics, University of Oxford, 1 Keble Road, Oxford OX1 3NP, UK

We calculate the flux of high energy γ -rays from annihilation of neutralino dark matter in the centre of the Milky Way and the two nearest dwarf spheroidals (Sagittarius and Draco), using realistic models of the dark matter distribution. Other investigators have used cusped dark halo profiles (such as the Navarro-Frenk-White) to claim a significant signal. This ignores the substantial astrophysical evidence that the Milky Way is not dark-matter dominated in the inner regions. We show that the annihilation signal from the Galactic Centre has accordingly been overestimated by at least two orders of magnitude. Thus the present and future generation of high energy γ -ray detectors, whether atmospheric Cerenkov telescopes or space missions like GLAST, lack the sensitivity to detect any of the monochromatic γ -ray annihilation lines. We show that the diffuse γ -ray signal may however be detectable and that the best prospect is the Sagittarius dwarf spheroidal.

I. INTRODUCTION

The foremost candidate for the cold dark matter (CDM) composing galactic haloes is the lightest neutral supersymmetric particle, namely the neutralino [1]. If so, then neutralino pair annihilation may lead to observable consequences, in particular the emission of high energy γ -radiation [2]. The possibility that such γ -rays may be identified by forthcoming atmospheric Cerenkov telescopes (ACT) such as VERITAS [3] or by satellite-borne detectors like GLAST [4] has excited considerable recent interest [5, 6, 7].

It is clearly of importance to identify the best places to search for such an annihilation signal. Inspired by the highly cusped models based on numerical simulations of dark halo formation [8, 9], a number of investigators have suggested that the centre of the Milky Way Galaxy may be the optimum target. For example, Bergstrom et al. [2] have shown that if the dark matter density is cusped as $1/r$ at small radii, then the γ -ray flux would be detectable for typical neutralino properties in the minimal supersymmetric extension of the Standard Model (MSSM). Inspired also by the persistence of substructure in numerical simulations, a number of authors [5, 10, 11] have argued that a substantial enhancement in the γ -ray signal can be expected from such ‘clumps’. In these calculations, the inner regions of the substructure are also usually assumed to be cusped. However, even within the framework of the cusped models favored by cosmological simulations, these conclusions have been contested as being overly optimistic [6].

More awkwardly, there is a substantial body of astrophysical evidence that the halo of the Milky Way Galaxy is not cusped at all [12]. First, the microlensing optical depth towards the Galactic Center is very high. Particle dark matter does not cause microlensing, whereas faint stars and brown dwarfs do. The total amount of all matter within the Solar circle is constrained by the rotation curve, so this tells us that lines of sight towards the Galactic Center are not dominated by particle dark matter. More specifically, haloes as strongly cusped as $1/r$, normalised to the local dark matter density as inferred from the stellar kinematics in the solar neighbourhood, are ruled out by the high microlensing optical depth [13]. Second, the pattern speed of the Galactic bar is known to be fast from hydrodynamical modelling of the motions of neutral and ionised gas. If dark matter dominates the central regions of the Milky Way, then dynamical friction will strongly couple the dark matter to the Galactic bar and cause it to decelerate on a few bar rotation timescales [14]. It is now largely accepted by astronomers that bright galaxies like the Milky Way do not have cusped dark haloes today, with some investigators suggesting that feedback from star formation may provide a resolution with cold dark matter theories [15].

In fact, there is *no* observational evidence whatsoever that any nearby galaxy has a cusped dark halo profile. The rotation curves of low surface brightness and dwarf spiral galaxies have been the subject of a long controversy [16, 17]. The effects of beam smearing mean that the H I rotation curves of many dwarf spirals are broadly compatible with both cores and cusps. However, the H II rotation curves for at least some dwarf spirals are not compatible with cusps [18]. Most dwarf spheroidals (dSphs) do not contain gas and so the structure of the dark halos must be inferred from stellar motions. Very recently, the survival of kinematically cold substructure in the Ursa Minor dSph has been used to argue against a cusped halo [19]. Hence, even at the least massive and most dark matter dominated end of the galaxy mass spectrum, the predictions of cold dark matter theories concerning halo structure seem to disagree with the observations. Nonetheless, for the two nearest dSphs – Draco and Sagittarius – there is no direct evidence either for or against central cusps in their dark matter distribution.

Given this weight of evidence, it seems very prudent to use both cored and cusped halo models to estimate the range of the expected γ -ray annihilation signal. In this paper, we examine three possible locations – the Galaxy Center and the centers of the two nearest dark-matter dominated dwarf spheroidals (Draco and Sagittarius).

In Section II we use the most recent data on the velocity dispersion of the dSphs to constrain a variety of dark halo models, and in Section III evaluate the γ -ray flux from neutralino self-annihilations. Sections IV and V summarise the expected contribution from the background and the criterion for detection respectively. The results for second generation ACTs and for GLAST are given in Section VI.

II. MODELS OF DWARF SPHEROIDALS

Dwarf spheroidals warrant attention because they are amongst the most extreme dark matter dominated environments. For example, the mass-to-light ratio of Draco is ~ 250 in Solar units [20], while that of the Sagittarius is ~ 100 [21]. Given the seeming absence of dark matter in globular clusters, dSphs are also the smallest systems dominated by dark matter.

We develop two sets of models of dSphs. The first set is the cored spherical power-law models [22]:

$$\rho_{\text{pow}}(r) \equiv \frac{v_a^2 r_c^\alpha}{4\pi G} \frac{3r_c^2 + r^2(1-\alpha)}{(r_c^2 + r^2)^{2+\alpha/2}}. \quad (1)$$

Here, r_c is the core radius and v_a is a velocity scale. When $\alpha = 0$, the model has an asymptotically flat rotation curve and is the cored isothermal sphere. The rotation curves of dwarf galaxies may be gently rising or falling at large radii, so we also consider models with $\alpha = -0.2$ and 0.2 respectively.

The second set of models is the cusped haloes

$$\rho_{\text{cusp}}(r) \equiv \frac{A}{r^\gamma (r + r_s)^{3-\gamma}}, \quad (2)$$

favored by numerical simulations. Here, r_s is the scale radius and A is the overall normalisation. When $\gamma = 1.5$, the model is the highly cusped Moore et al. [8] profile, when $\gamma = 1$, the model is the Navarro-Frenk-White (NFW) profile [9]. Additionally, we study the case $\gamma = 0.5$ which represents a still milder cusped profile.

The two free parameters determining the shape of the profile are set by fitting to observational data on the Draco dSph using the Jeans equation [23]. For a spherical galaxy, the enclosed mass $M(r)$ is related to observables via

$$M(r) = -\frac{r\langle v_r \rangle^2}{G} \left(\frac{d \log \nu}{d \log r} + \frac{d \log \langle v_r^2 \rangle}{d \log r} + 2\beta \right). \quad (3)$$

Here, ν is the luminosity density, $\langle v_r^2 \rangle$ is the radial velocity dispersion of the stars and β is the anisotropy of the stellar motions. The luminosity density of Draco ν is taken as [24]:

$$\nu = \frac{\nu_0 r_0^5}{(r_0^2 + r^2)^{5/2}}, \quad (4)$$

with $r_0 = 9.71' \approx 0.23$ kpc (using a heliocentric distance for Draco of 82 kpc). There are 6 observational points showing the line of sight velocity dispersion of Draco at different radii in [25] (using the data with no rotation subtracted). The datapoints are consistent with a flat profile between radii of $2'$ and $22'$. Assuming that the anisotropy now vanishes, then the radial velocity dispersion is equal to the line of sight velocity dispersion. Finally, the left-hand side of eq. (3) is fitted to the known right-hand side at the locations of the datapoints in [25], thus giving the two unknown parameters for each density profile quoted in Table I.

This algorithm provides models of the Draco dSph that satisfy the available observational data. Unfortunately, the radial variation of the velocity dispersion has not been measured for the Sagittarius dSph. However, the central line of sight velocity dispersion of Sagittarius dSph is 11.4 kms^{-1} , very similar to that of Draco (10 kms^{-1}). Henceforth, we assume that the underlying structural parameters (v_a, r_c or A, r_s) of Sagittarius are the same as Draco.

To determine the extent of the dark matter halo of the dSphs, the tidal radius must be estimated. The approximate method used conventionally is derived from the Roche criterion. The tidal radius is found by requiring that the average mass in the dSph is equal to the average interior mass in the Milky Way galaxy, namely

$$\frac{M_{\text{dSph}}(r_t)}{r_t^3} = \frac{M_{\text{MW}}(r_{\text{dSph}} - r_t)}{(r_{\text{dSph}} - r_t)^3}. \quad (5)$$

Here, r_{dSph} is the distance from the Galactic Center to the centre of the dSph. We remark that this is not the same as the procedure used in a number of recent papers [7, 26, 27], in which the local density at the tidal radius in the dSph is set equal to the density of the background Milky Way halo at the center of the dSph.

Cored Power-Law Models					
α	v_a kms $^{-1}$	r_c kpc	r_t kpc MW - Iso	r_t kpc MW - NFW	$M(r_t) \times 10^8 M_\odot$
0.2	24.7	0.25	6.2 (2.16)	1.3 (0.5)	4.6 (2.0)
0	22.9	0.23	7.8 (2.5)	1.4 (0.51)	9.5 (3.0)
-0.2	20.9	0.21	10.1 (2.8)	1.6 (0.52)	22.43 (4.9)

Cusped Models					
γ	$A \times 10^7 M_\odot$	r_s kpc	r_t kpc MW - Iso	r_t kpc MW - NFW	$M(r_t) \times 10^8 M_\odot$
0.5	2.3	0.32	6.6 (2.5)	1.5 (0.6)	5.5 (3.1)
1 (NFW)	3.3	0.62	7.0 (2.59)	1.6 (0.57)	6.6 (3.5)
1.5 (Moore)	2.9	1.	6.5 (2.4)	1.5 (0.6)	5.5 (2.8)

TABLE I: Parameters of the dark matter halo profiles of the Draco dSph. The last three columns give (in parentheses) the values at the location of Sagittarius dSph. Two values are given for the tidal radius, according to whether the Milky Way Galaxy is modelled with an isothermal power-law model or a NFW model. [Notes: (1) the models require a slight velocity anisotropy in the very innermost parts to ensure everywhere physical stresses in the Jeans equation, (2) the scale radius r_s is constrained to lie below 1 kpc].

mSUGRA parameters

m_0 (GeV)	$m_{1/2}$ (GeV)	$\tan \beta$	$ A_0 $ (GeV)
10-10000	10-10000	1-60	10-10000

TABLE II: This shows the portion of the mSUGRA parameter space randomly scanned. Here, m_0 and $m_{1/2}$ are respectively the common scalar mass and gaugino mass at the unification scale, while A_0 is the trilinear parameter and $\tan \beta$ is the ratio of the vacuum expectation values of the two Higgs fields. The μ term in the super-symmetric Lagrangian is allowed to have either sign.

The results depend on the choice of profile for the Milky Way Galaxy. For comparison purposes, we use a NFW profile with concentration parameter $c = 10$ and a cored isothermal profile with $r_c = 10$ kpc and $v_a = 220$ kms $^{-1}$. The total mass of the Milky Way Galaxy is fixed at $M_{\text{MW}} = 10^{12} M_\odot$, as suggested in [28]. We show in Table I the results when eq. (5) is used to determine the tidal radius for the models of the Milky Way Galaxy.

III. THE GAMMA-RAY FLUX

Let the neutralino mass be m_χ and its self-annihilation cross-section be $\langle \sigma v \rangle$. Then, the γ -ray flux from neutralino annihilation is given by [2]

$$\Phi_\gamma(\psi) = \frac{N_\gamma \langle \sigma v \rangle}{4\pi m_\chi^2} \times \frac{1}{\Delta\Omega} \int_{\Delta\Omega} d\Omega \int_{\text{los}} \rho^2(r(s)) ds, \quad (6)$$

where ρ is the density of the dSph as a function of distance from its center r , which of course depends on the heliocentric distance s . The integration is performed along the line of sight to the target and averaged over the solid angle $\Delta\Omega$ of the detector. In particular, $N_\gamma = 2$ for the annihilation of two nonrelativistic neutralinos into two photons ($\chi\bar{\chi} \rightarrow \gamma\gamma$) and $N_\gamma = 1$ for the annihilation into a photon and a Z boson ($\chi\bar{\chi} \rightarrow Z\gamma$). The first part of the integrand (6) depends on the particular particle physics model for neutralino annihilations. The second part is a line of sight integration through the dark matter density distribution. We discuss each in detail in the next two subsections.

A. Particle Physics Model

To compute $N_\gamma \langle \sigma v \rangle / (4\pi m_\chi^2)$, we have to select a supersymmetric model. We focus on minimal supergravity (mSUGRA) models with universal gaugino and scalar masses and trilinear terms at the unification scale. We use the

computer programme SoftSusy [29] to scan the supersymmetric parameter space (see Table II) and generate $\sim 10^5$ models which have consistent electroweak symmetry breaking and grand unification. The output at the electroweak scale is fed into the programme DarkSusy [30] which computes the relic density and products of the neutralino annihilations. It also checks that a given model is not ruled out by present accelerator experiments.

A feasible model is one which is permitted by accelerator limits and which predicts a relic density in the range $0.005 < \Omega_{\text{CDM}} h^2 < 0.2$. This upper limit is slightly greater than the value determined by fitting the standard ΛCDM model to the WMAP data [31]. This is done so as to incorporate the higher values found for pure CDM models [32]. The lower limit is set by requiring the relic particle to provide most of the dark matter. Taking a typical mass to light ratio for galaxies of ~ 10 , then $\Omega_{\text{CDM}} h^2 \sim 0.005$ for a critical mass to light ratio of ~ 2000 in solar units. The range of the supersymmetric parameters scanned are given in Table II. For each feasible model, we record the quantities $N_\gamma \langle \sigma v \rangle$ for the discrete lines $\chi\chi \rightarrow \gamma\gamma$ and $\chi\chi \rightarrow Z\gamma$, as well as the continuous γ -ray spectrum above 1 and 50 GeV. Note that in previous studies, such as [2], the relic density is much less constrained and models with an arbitrary low value are permitted.

B. Line of Sight Integration of Dark Matter Density

The line of sight integration can be manipulated thus:

$$\langle J(0) \rangle_{\Delta\Omega} \doteq \frac{1}{\Delta\Omega} \int_{\Delta\Omega} J(\psi) d\Omega = \frac{2\pi}{\Delta\Omega} \int_0^{\theta_{\max}} d\theta \sin\theta \int_{s_{\min}}^{s_{\max}} ds \rho^2(\sqrt{s^2 + s_0^2 - 2ss_0 \cos\theta}) \quad (7)$$

where

$$J(\psi) = \int_{\text{los}} ds \rho^2(r). \quad (8)$$

In these formulae, angled brackets denote the averaging over the solid angle $\Delta\Omega$, while s_{\min} and s_{\max} are the lower and upper limits of the line of sight integration, given by $s_0 \cos\theta \pm \sqrt{r_t^2 - s_0^2 \sin^2\theta}$. Here, s_0 is the heliocentric distance of the dSph and r_t is the tidal radius of the dSph. Finally, θ_{\max} is the angle over which we average around the center of the dSph. It generally is, at least, equal to the experimental resolution and can be fixed using:

$$\Delta\Omega = 2\pi \int_0^{\theta_{\max}} d\theta \sin\theta = 2\pi(1 - \cos(\theta_{\max})).$$

The quoted point spread function widths for the various experiments are: 0.4° (EGRET), 0.1° (GLAST, HESS and VERITAS), $0.15^\circ - 0.04^\circ$ (CANGAROO-III). EGRET and GLAST are satellite detectors with low energy thresholds (≈ 100 MeV), high energy resolution ($\approx 15\%$) but worse angular precision. The others are ACTs with higher thresholds (≈ 100 GeV) but better angular resolution. Typical reference sizes for the solid angle are $\Delta\Omega = 10^{-5}$ sr for ACTs and GLAST and $\Delta\Omega = 10^{-3}$ sr, which is close to the EGRET value.

Table III lists values of $\langle J(0) \rangle_{\Delta\Omega}$ for the dSph profiles introduced in Section II. The signal for Sagittarius is always larger than that for Draco. An increase in angular sensitivity enhances the signal for both Sagittarius and Draco. We remark that, in the literature, there is a considerable spread in the values obtained for $\langle J(0) \rangle_{\Delta\Omega}$ for different sources. In [33], a 1-component King profile was used to model the dSph density distribution. These authors only give explicit estimates of the entire line-of-sight integral. However, the values are of the order of $10^{21} \text{ GeV}^2 \text{ cm}^{-5}$, lower than those implied by Table III. In [7], no angular average is taken, but instead the approximation

$$J \approx \frac{\int_{\text{los}} \rho^2(l) dl}{4\pi d^2}, \quad (9)$$

is used, together with an (unrealistic) singular isothermal profile for Draco. Taking the value given for $m_\chi = 100$ GeV implies $3.7 \times 10^{20} \text{ GeV}^2 \text{ cm}^{-5}$ for the line-of-sight integral. It is surprisingly low and yet the plots manage to exclude as large a region in parameter space as in [2]! As we discuss in Section V, the reason for this is the criterion used in [7] to identify a detectable signal.

The γ -ray emission towards the Galactic Center falls by at least two orders of magnitude on moving from a cusped NFW halo to a cored isothermal model. In [2], an optimistic result for the γ -ray flux towards the Galactic Center was obtained by using a cusped NFW model normalised to lie within two constraints on the halo mass M and circular speed v_h , namely

$$M(r < 100 \text{ kpc}) = (6.3 \pm 2.5) \times 10^{11} M_\odot, \quad v_h(R_0) \approx 128 - 207 \text{ km s}^{-1} \quad (10)$$

Cored Power-Law Models

α	Sagittarius		Draco	
	$\Delta\Omega = 10^{-3}$ sr	$\Delta\Omega = 10^{-5}$ sr	$\Delta\Omega = 10^{-3}$ sr	$\Delta\Omega = 10^{-5}$ sr
0.2	0.6	3.4	0.07	2.2
0	0.6	3.3	0.06	2.2
-0.2	0.6	3.2	0.07	2.2

Cusped Models

γ	Sagittarius		Draco	
	$\Delta\Omega = 10^{-3}$ sr	$\Delta\Omega = 10^{-5}$ sr	$\Delta\Omega = 10^{-3}$ sr	$\Delta\Omega = 10^{-5}$ sr
0.5	1.1	17.8	0.1	5.7
1 (NFW)	1.3	36.9	0.1	7.2
1.5 (Moore)	7.3	615.1	0.6	55.4

Galactic Center

Profile	$\Delta\Omega = 10^{-3}$ sr	$\Delta\Omega = 10^{-5}$ sr
NFW, $\gamma = 1$	26.	280.
Cored, $\alpha = 0$	0.3	0.3

TABLE III: Values of $\langle J(0) \rangle_{\Delta\Omega}$ for the Sagittarius and Draco dSphs in units of $10^{23} \text{ GeV}^2 \text{ cm}^{-5}$. The tidal radius of the dSphs is calculated assuming an isothermal profile for the galaxy. Additionally, results in the direction of the Galactic Center for the two models of the Milky Way are also given.

If the normalisation is set to obtain the maximum flux (as is done for example in Fig. 9 of [2]), then the models possess a local dark matter density substantially in excess of the usual value of $\sim 0.3 \text{ GeV cm}^{-3}$. Anyhow, even accepting the debatable proposition that the Galaxy did once have a pristine dark halo of the NFW form, the formation of the Galactic disk, bulge and bar will have substantially re-processed the dark matter distribution. Certainly, the evidence from the microlensing optical depth towards the Galactic Centre and the pattern speed of the Galactic bar are inconsistent with models dominated by dark matter in the central regions [12].

IV. COMPUTATION OF THE BACKGROUND

There are three sources of background for the signal under consideration: hadronic, cosmic-ray electrons and diffuse γ -rays from astrophysical processes. The last is negligible for ACTs, but is the only one present for satellite experiments like GLAST or EGRET. Let us consider each source of background in turn.

A. Hadronic and Electronic

Bergstrom et. al. [2] use data taken with the Whipple ACT to derive the following expression for the hadronic background:

$$\frac{d\Phi_{\text{had}}}{d\Omega} (E > E_0) = 6.1 \times 10^{-3} \epsilon_{\text{had}} \left(\frac{E_0}{1 \text{ GeV}} \right)^{-1.7} \text{ cm}^{-2} \text{ s}^{-1} \text{ sr}^{-1}, \quad (11)$$

where ϵ_{had} is intended to take into account improved hadronic rejection expected in future ACTs, but is at present set to unity.

Showers initiated by cosmic-ray electrons are indistinguishable from gamma rays. This contribution to the background for ACTs is, according to [2] (who cite [34] for this purpose):

$$\frac{d\Phi_{e^-}}{d\Omega} = 3.0 \times 10^{-2} \left(\frac{E_0}{1 \text{ GeV}} \right)^{-2.3} \text{ cm}^{-2} \text{ s}^{-1} \text{ sr}^{-1}. \quad (12)$$

B. Diffuse Emission

The diffuse γ -ray background is usually taken to be dominated by the Galactic [35] or extragalactic [36] contribution, depending on whether the target location is the Galactic Center or at higher latitudes ($b \geq 10^\circ$). For example, a fit to the EGRET data [35] at 1 GeV (dominated by the Galactic contribution) is given in [2] as

$$\frac{d\Phi_{\text{diff}}}{d\Omega dE} = N_0(l, b) 10^{-6} \left(\frac{E_0}{1 \text{ GeV}} \right)^{-2.7} \text{ cm}^{-2} \text{ s}^{-1} \text{ sr}^{-1} \text{ GeV}^{-1}, \quad (13)$$

where $N_0(l, b)$ is a factor in the range 1-100, with higher values for the central regions of the Galaxy. In [33], only the extragalactic contribution from EGRET, estimated in [36], is considered:

$$\begin{aligned} \frac{d\Phi_{\text{diff}}}{d\Omega dE} &= (7.32 \pm 0.34) \times 10^{-9} \left(\frac{E_0}{451 \text{ MeV}} \right)^{-2.10 \pm 0.03} \text{ cm}^{-2} \text{ s}^{-1} \text{ sr}^{-1} \text{ MeV}^{-1} \\ &\approx 1.4 \times 10^{-6} \left(\frac{E_0}{1 \text{ GeV}} \right)^{-2.10 \pm 0.03} \text{ cm}^{-2} \text{ s}^{-1} \text{ sr}^{-1} \text{ GeV}^{-1}. \end{aligned} \quad (14)$$

So, the spectral indices of the Galactic and extragalactic contributions are about -2.7 and -2.1 respectively.

However, the separation between the Galactic and extragalactic background is not clear. For example in [37], the case is made for a very low extragalactic background. Studying the region around the Galactic poles ($b \approx 90^\circ$), it is concluded that, even there, most of the contribution is of Galactic origin. In particular, it is shown that the main contribution is not isotropic but correlated with known Galactic tracers. The EGRET collaboration concede that *any* simple model for the diffuse background is unlikely to work for all points in the sky and at all energies [38].

To be conservative, we normalize the flux to the EGRET data above 1 GeV and choose a spectral index of -2.1 which is the worst case:

$$\frac{d\Phi_{\text{diff}}}{d\Omega dE} = \mathcal{N} \left(\frac{E}{1 \text{ GeV}} \right)^{-2.1}. \quad (15)$$

The emission above 1 GeV in the region of our interest can be downloaded from the EGRET website [39]. The exact values for the diffuse emission are $6.7 \times 10^{-7} \text{ cm}^{-2} \text{ s}^{-1} \text{ sr}^{-1}$ at the location of the Draco dSph ($l = 86.4^\circ$, $b = 34.7^\circ$), $3.18 \times 10^{-6} \text{ cm}^{-2} \text{ s}^{-1} \text{ sr}^{-1}$ at the location of the Sagittarius dSph ($l = 5.6^\circ$, $b = -14.1^\circ$) and $1.2 \times 10^{-4} \text{ cm}^{-2} \text{ s}^{-1} \text{ sr}^{-1}$ at the Galactic Center.

The diffuse emission is the only background for satellite experiments. Its large variation with Galactic coordinates can make a weak source in Draco relatively brighter than strong emission from the Galactic Center, overwhelming the fluxes in Table III. For ACTs, however, the hadronic and electronic backgrounds are much larger and independent of Galactic coordinates, so the hierarchy from Table III is retained. So, this raises the possibility that the Sagittarius dSph might have a higher signal-to-noise ratio with ACTs, but the Draco dSph is more clearly seen from satellites.

V. THE DETECTORS

A. Minimum Detectable Flux

For the Sagittarius and Draco dSphs, the minimum detectable flux Φ_γ is determined using the prescription that, for an exposure of t seconds made with an instrument of effective area A_{eff} and angular acceptance $\Delta\Omega$, the significance of the detection should exceed 5σ and the number of detected photons be larger than 25:

$$\frac{\Phi_\gamma \times \Delta\Omega A_{\text{eff}} t}{\sqrt{A_{\text{eff}} t} \sqrt{\frac{d\Phi_{\text{bg}}}{d\Omega} \times \Delta\Omega}} \geq 5, \quad \Phi_\gamma A_{\text{eff}} t \geq 25. \quad (16)$$

Here, Φ_γ denotes a flux in $\text{cm}^{-2} \text{ s}^{-1} \text{ sr}^{-1}$, whereas N denotes photon counts and so $N \equiv \Phi_\gamma \times \Delta\Omega A_{\text{eff}} t$.

When studying the signal from discrete γ -lines, $d\Phi_{\text{bg}}/d\Omega$ is the background flux falling under the annihilation line. If the background has a differential spectrum $d^2\Phi_{\text{bg}}/d\Omega dE = N_0 E^{-\delta}$, and if the energy resolution of the instrument is σ_E/E , then the background under a line at energy E_0 (i.e., in the interval $[E_0 - \sigma_E, E_0 + \sigma_E]$ containing 68% of the signal) is given by [2]:

$$\frac{d\Phi_{\text{bg}}}{d\Omega} = \frac{N_0}{\delta - 1} E_0^{-\delta+1} \times \eta(\sigma_E/E, \delta), \quad (17)$$

with

$$\eta(\sigma_E/E, \delta) = \frac{1}{(1 - \sigma_E/E)^{1-\delta}} - \frac{1}{(1 + \sigma_E/E)^{1-\delta}}. \quad (18)$$

For ACTs, the background is the sum of three different power laws.

The critical number of detected photons chosen in eq. (16) is somewhat arbitrary. This is demonstrated by the range of values used in the literature. In [2], it is lowered from 25 to 10 when considering satellite experiments; in [40], it is taken to be 100 for ACTs; in [33], no minimum number of detected photons is required. In [7], a completely different strategy altogether is used: constraints on supersymmetric parameter space are found by requiring that Draco's flux be less than the least significant detection (the Large Magellanic Cloud at 4σ [41]) above 1 GeV, resulting in a minimum flux for detection of $10^{-8} \text{ cm}^{-2} \text{s}^{-1}$. In this way, the noise enters *linearly* into the expression. This explains why Tyler [7] excludes a large region in mSUGRA parameter space from the non-detection of dSphs, despite the fact that the values of the integral (7) towards the dSphs are quite low.

B. Performance of the Detectors

The detector characteristics of the different experiments are summarised in Table IV. For definiteness, we use $\Delta\Omega = 10^{-5} \text{ sr} \approx 0.1^\circ$ for the angular average when considering ACTs or GLAST, and $\Delta\Omega = 10^{-3} \text{ sr} \approx 1^\circ$ for EGRET. Also important is the observation time, which is chosen as $t \approx 1 \text{ yr}$ for satellites. For the next generation ACTs, assuming four telescopes, we use an observation time $t \approx 100 \text{ h}$ and an exposure $A_{\text{eff}} = 4 \times 10^8 \text{ cm}^2$. This seems reasonable, as CANGAROO [42] and the last phase of HESS [43] will have four telescopes, while VERITAS will have as many as seven [3]. MAGIC [44] uses a single 17m mirror and has roughly the same performance as next-generation ACTs, but with a reduced threshold of 30 GeV.

VI. RESULTS

The following plots show the parts of the supersymmetric parameter space that can be excluded from the lack of a detectable γ -ray signal from neutralino annihilations. We typically show the region excluded by EGRET, GLAST and a generic second generation ACT. The type of plots found in [2] show the γ -ray flux in $\text{cm}^{-2} \text{s}^{-1}$ against photon energy. They are not appropriate for depicting the exclusion limits from observations of different parts of the sky because the flux changes and hence so do the points representing theoretical models. We prefer to use the type of plot presented in [33] with $N_\gamma \langle \sigma v \rangle$ (which depends exclusively on the particle physics model) versus m_χ (although other quantities could be used as well).

From eq. (16), we write the condition for detection in a more convenient way for the plots:

$$N_\gamma \langle \sigma v \rangle \geq 5 \sqrt{\frac{d\Phi_{\text{bg}}}{d\Omega} \Delta\Omega} \frac{1}{\sqrt{A_{\text{eff}} t}} \frac{4\pi m_\chi^2}{\Delta\Omega \langle J \rangle} \quad N_\gamma \langle \sigma v \rangle \geq \frac{25}{A_{\text{eff}} t} \frac{4\pi m_\chi^2}{\Delta\Omega \langle J \rangle}. \quad (19)$$

Here, we see that increasing the angular acceptance $\Delta\Omega$ could increase the signal to noise ratio. In fact, if we take both signal and background to be constant, the significance increases (and the minimum value of $N_\gamma \langle \sigma v \rangle$ that can be probed decreases) as $\sqrt{\Delta\Omega}$, so the optimal strategy is to analyze the photons in the *full* field of view of the detector centered in the source (after of course subtracting other point sources). The signal is not constant as Table III shows, but the angular acceptance that maximizes the significance does not necessarily coincide with the minimum angular resolution of the detector. So, instead of using the numbers there, we compute the angle for which the signal to noise ratio is maximised. The angle depends on the position and on the type of profile. For instance, Draco, being very far away, looks like a point source and the maximum signal is for the smallest angle possible. For Sagittarius, the optimal angle is 0.4° for cored profiles and the smallest possible for cusped profiles. In order not to put too many lines in the plot, we have avoided drawing all the halo types and show only the extreme cases.

A. Discrete Lines

The annihilation of two neutralinos gives rise to two photons with energy $E_\gamma \approx m_\chi$. The region probed by the different experiments is shown in Fig. 1. Also shown are ~ 1500 points in the mSUGRA parameter space that comply with all the accelerator limits (including $b \rightarrow s\gamma$, $(g-2)_\mu$ and other accelerator limits [45] that are incorporated in

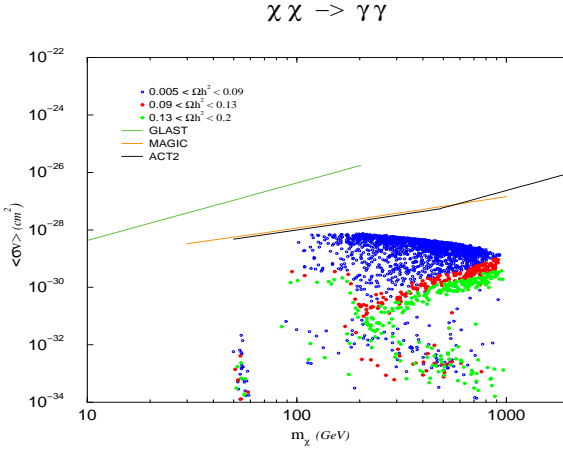


FIG. 1: Exclusion limits for the discrete line $\chi\chi \rightarrow \gamma\gamma$ exclusion plots. For all the experiments, only the most favorable case (that of Sagittarius dSph with a Moore profile) is shown. All points satisfy $0.005 < \Omega_{\text{CDM}}h^2 < 0.2$. The red points are in accord with the WMAP constraints. The exclusion limits for $\chi\chi \rightarrow Z\gamma$ are very similar and not shown.

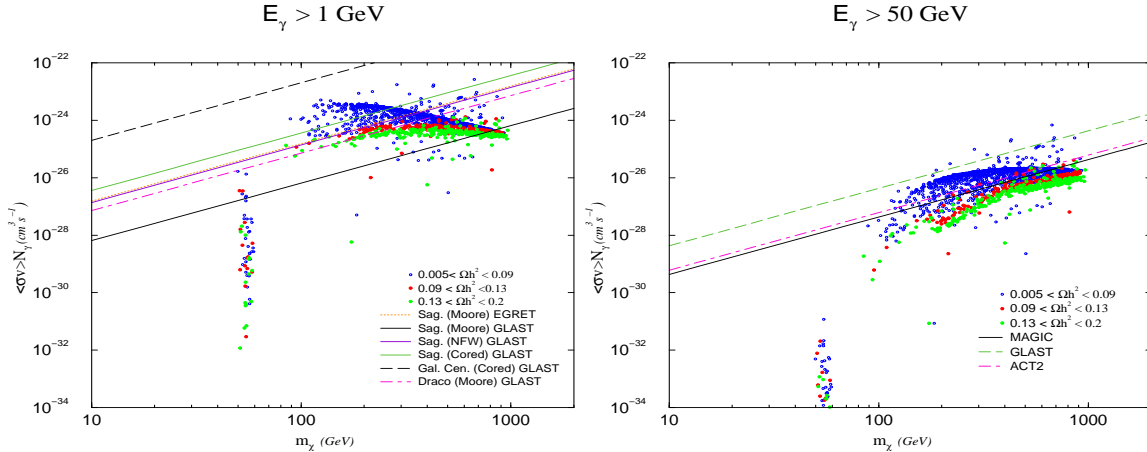


FIG. 2: Exclusion limits for continuum γ -ray emission above 1 GeV (left) and 50 GeV (right). All points satisfy $0.005 < \Omega_{\text{CDM}}h^2 < 0.2$. The red points are in accord with the WMAP constraints.

DarkSusy). All the points, bar five, have spin-independent cross-section with protons or neutrons below 10^{-6} pb, thus compatible with limits set by the Edelweiss nuclear recoil detector, but not the disputed signal claimed by the DAMA experiment [46]. Also, the upward-going, neutrino originated, muon showers have a rate from the Earth or Sun of $\leq 10^4$ km 2 yr $^{-1}$ (which according to Kurylov and Kamionkowski [47] is the limit set by super-Kamiokande).

As the figure shows, the discrete annihilation line is very unlikely to be observed, even with the next generation instruments. Even for the most promising target – the Sagittarius dSph galaxy assuming a Moore profile – the flux is too low. The other possible models and targets (such as the Galactic Center) lie above the lines for the Sagittarius and are thus still less propitious. The difference between this work and that of [2] is that the latter authors took a very high dark matter concentration in the center (the profile is just NFW, but the constant in front is set to ensure maximal flux given two weak constraints on the mass and the rotation curve).

B. Continuum Emission

The continuum emission comes from hadronization and subsequent pion decay. The programme DarkSusy [30] uses results from the PYTHIA Monte Carlo to compute the photon multiplicity for each neutralino annihilation. Experimental sensitivities are shown in Fig. 2 for continuum emission above 1 GeV and 50 GeV.

The continuum emission above 1 GeV (and even above 50 GeV) can yield some constraints. Although we have computed the curves for three targets (Draco, Sagittarius and the Galactic Centre) and for the full range of models in Section II, we give only the most promising results in the figures. The Draco and Sagittarius dSphs may yield interesting constraints — but only if their dark halo profiles are strongly cusped. Unlike the case of the Milky Way, cusped profiles are still possible for the dSphs. Notice, however, that substituting cored isothermal-like models for NFW or Moore profiles causes the exclusion limit to move well above the supersymmetric parameter space of interest.

VII. CONCLUSIONS

If the dark matter present in the Universe is composed at least in part by the lightest supersymmetric particle, then this could manifest itself via γ -ray emission from pair annihilations. It is clearly important to estimate the likely size of the neutralino annihilation signal. It is also important to identify the likely locations and spectral régimes in which the signal should be sought. This paper has provided new estimates of the signal towards the Galactic Center and the nearby dwarf spheroidals using a variety of models.

There have been a number of recent calculations predicting that the neutralino annihilation flux from the inner Galaxy will be detectable with forthcoming satellites like GLAST and with second generation atmospheric Cerenkov telescopes (ACTs) [2, 6]. These calculations assume that the cusped Navarro-Frenk-White (NFW) models for the Galaxy halo hold good. This assumption is in contradiction with a substantial body of astrophysical evidence about the inner Galaxy [12, 13, 14]. In any case, even if the Galaxy halo was originally of NFW form, the formation of the disk and bulge will have reprocessed the primordial dark matter distribution [15]. In contradiction with earlier results, we do not find the prospects of detecting the annihilation flux from the Galactic Center to be particularly promising. In particular, the γ -ray line coming from the $\gamma\gamma$ and $Z\gamma$ final states is not detectable either with second generation ACTs or with the GLAST satellite. *We caution that many of the recent estimates of high flux are sensitively dependent on the assumptions made regarding the innermost structure of the dark halo. Even the best numerical simulations have difficulty in resolving structures on scales less than 1 kpc, and so the inner profile is always found by extrapolation.*

The high mass-to-light ratios of the Local Group dwarf spheroidals (dSphs) makes them possible targets. Cusped profiles like NFW are not presently ruled out for dSphs like Sagittarius or Draco. It may be that the visible dwarf galaxy lies entirely within the central parts of a cusped dark matter halo. If so, then the optimum target is the Sagittarius dSph. The detection of monochromatic lines is still extremely difficult, but the GLAST satellite may detect excess continuum γ ray emission. This is of course a less distinctive feature than a sharp line. In particular, if the Sagittarius has a strongly cusped dark halo profile ($\rho \sim r^{-1.5}$), then large regions of supersymmetric parameter space can be ruled out. Again, however, this conclusion only holds good if the dark halo profile is cusped. Using a cored isothermal-like model for the dark halo, even the Sagittarius dSph will be invisible to GLAST and second generation ACTs.

Unlike Bergstrom et al. [2], we do not find the Galactic Center to be a promising location. Partly, this is because we believe that the Milky Way does *not* have a strongly cusped profile based on the available astrophysical evidence [12, 13, 14]. Partly, this is because Bergstrom et al. chose a generous overall normalisation anyhow — they used the NFW model corresponding to the maximum flux which satisfies two weak constraints on the mass and the rotation curve. Accordingly, the local dark matter density is as high as ~ 0.6 GeV cm $^{-3}$ in their model. When the circular velocity curve of such a halo is combined with that for the disk and bar, then it necessarily violates the constraint on the Galactic rotation curve in the inner parts. One important caveat of our results — however — is that the possible effects of a central black hole are not included in our calculations. Here, we merely note that the observability of any expected signal depends on the manner in which the black hole grows [49, 50].

Very recently, the Large Magellanic Cloud (LMC) has been suggested as another likely target [27]. Judging from [48], the average mass to light ratio of the LMC within 8.9 kpc is only ~ 3 (as opposed to ~ 100 for the compact dSphs). This is an upper limit to the central mass to light ratio. In other words, much like the Milky Way Galaxy, dark matter dominates the outer parts of the LMC and is responsible for the asymptotic flatness of the ratio curve. However, the central parts of the LMC are dominated by the luminous bar and disk. The assumption that the dark halo dominates the gravitational potential everywhere is therefore not valid. Hence, the procedure used in [27] of fitting the rotation curve to a NFW dark halo is flawed. The gravitational potential of the gas and stellar disk and bar simply cannot be ignored in the central regions.

Acknowledgments

We are grateful to M. Martinez, M. Ramage and C. Tyler for useful correspondence.

[1] G. Jungman, M. Kamionkowski and K. Griest, Phys. Rep. **267** (1996) 195.

[2] L. Bergström, P. Ullio and J. H. Buckley, Astropart. Phys. **9** (1998) 137 [arXiv:astro-ph/9712318].

[3] <http://veritas.sao.arizona.edu/>

[4] <http://www-glast.stanford.edu/>

[5] J.E. Taylor and J. Silk, MNRAS **339** (2003) 505 [arXiv:astro-ph/0207299].

[6] F. Stoehr, S. D. White, V. Springel, G. Tormen and N. Yoshida, MNRAS, submitted [arXiv:astro-ph/0307026].

[7] C. Tyler, Phys. Rev. D **66** (2002) 023509 [arXiv:astro-ph/0203242].

[8] B. Moore, F. Governato, T. Quinn, J. Stadel and G. Lake, Astroph. J. **499** (1998) L5 [arXiv:astro-ph/9709051].

[9] J. F. Navarro, C. S. Frenk and S. D. White, Astroph. J. **490** (1997) 493 [arXiv:astro-ph/9611107].

[10] L. Bergström, J. Edsö, P. Gondolo and P. Ullio, Phys. Rev. **59** (1999) 043506 [arXiv:astro-ph/9806072].

[11] C. Cálcaneo-Roldan and B. Moore, Phys. Rev. D **62** (2000) 123005 [arXiv:astro-ph/0010056].

[12] N. W. Evans, In IDM 2000: The Third International Conference on the Identification of Dark Matter, eds N. Spooner, V. Kudraytsev, (World Scientific, Singapore), p.85 [arXiv:astro-ph/0102082].

[13] J. J. Binney and N. W. Evans, MNRAS **327** (2001) L27 [arXiv:astro-ph/0108505].

[14] V. Debattista and J. A. Sellwood, Astrophys. J. **493** (1998) L5 [arXiv:astro-ph/9710039].

[15] J. J. Binney, O. E. Gerhard and J. Silk MNRAS **321** (2001) 471 [arXiv:astro-ph/0003199].

[16] W. J. G. de Blok, S. S. McGaugh, A. Bosma and V. C. Rubin Astrophys. J. **552** (2001) L23 [arXiv:astro-ph/0103102].

[17] F. C. van den Bosch and R. A. Swaters, MNRAS, **325** (2001) 1017 [arXiv: astro-ph/0006048].

[18] S. Blais-Ouellette, C. Carignan, P. Amram and S. Côté, AJ **118** (1999) 2123 [arXiv:astro-ph/9911223].

[19] J. T. Kleyne, M. I. Wilkinson, G. Gilmore and N. W. Evans, Astrophys. J. **588** (2003) L21 [arXiv:astro-ph/0304093].

[20] J. T. Kleyne, M. I. Wilkinson, N. W. Evans and G. Gilmore Astrophys. J. **563** (2001) L115 [arXiv:astro-ph/0304093].

[21] R. A. Ibata, R. F. G. Wyse, G. Gilmore, M. J. Irwin, N. B. Suntzeff, Astron. J. **113** (1997) 634

[22] N. W. Evans, MNRAS **260** (1993) 191; MNRAS **267** (1994) 333

[23] J. Binney, S. Tremaine, “Galactic Dynamics”, Princeton University Press, 1987 (section 4.2).

[24] M. I. Wilkinson, J. Kleyne, N. W. Evans and G. Gilmore, MNRAS **330** (2002) 778 [arXiv:astro-ph/0109451]

[25] J. T. Kleyne, M. I. Wilkinson, N. W. Evans and G. Gilmore, MNRAS **330** (2002) 792 [arXiv:astro-ph/0109450].

[26] P. Blasi and R. Sheth, Phys. Lett. B **486** (2000) 233 [arXiv:astro-ph/0006316]

[27] A. Tasitsiomi, J. Gaskins and A. V. Olinto Phys. Rev. D (2003) submitted [arXiv:astro-ph/0307375]

[28] M. I. Wilkinson and N. W. Evans, MNRAS **310** (1999) 645 [arXiv:astro-ph/9906197].

[29] B. C. Allanach, arXiv:hep-ph/0104145, <http://allanach.home.cern.ch/allanach/softsusy.html>.

[30] P. Gondolo, J. Edsö, L. Bergstrom, P. Ullio and E. A. Baltz, <http://www.physto.se/~edsjo/darksusy/>.

[31] D. N. Spergel et al., Astrophys. J. (2003) in press [arXiv:astro-ph/0302209]

[32] A. Blanchard, M. Douspis, M. Rowan-Robinson and S. Sarkar, Astron. Astrophys. (2003) in press [astro-ph/0304237].

[33] E. A. Baltz, C. Briot, P. Salati, R. Taillet and J. Silk, Phys. Rev. D **61** (2000) 023514 [arXiv:astro-ph/9909112].

[34] M. S. Longair, “High energy astrophysics”, Cambridge University Press, 1992.

[35] S. D. Hunter et al., Astrophys. J. **481** (1997) 205.

[36] P. Sreekumar et al., Astrophys. J. **494** (1998) 523 [arXiv:astro-ph/9709257].

[37] U. Keshet, E. Waxman and A. Loeb, Astrophys. J. (2003) submitted [arXiv:astro-ph/0306442].

[38] R. C. Hartman et al. [EGRET Collaboration], Astrophys. J. Suppl. **123** (1999) 79.

[39] <http://cossc.gsfc.nasa.gov/egret/>

[40] F. A. Aharonian, W. Hofmann, A. .K. Konopelko and H. J. Völk, Astropart. Phys. **6** (1997) 369.

[41] R. C. Lamb and D. J. Macomb, Astrophys. J. **488** (1997) 872.

[42] <http://www.physics.adelaide.edu.au/astrophysics/cangaroo.html>

[43] <http://www.mpi-hd.mpg.de/hfm/HESS/HESS.html>

[44] <http://hegra1.mppmu.mpg.de/MAGICWeb/>; M. Martinez, Proc. of the XXVI ICRC **5** (1999) 219.

[45] K. Hagiwara et al. (Particle Data Group), Phys. Rev. D **66** (2002) 010001.

[46] <http://cdms.berkeley.edu/limitplots/>

[47] A. Kurylov and M. Kamionkowski, arXiv:hep-ph/0307185.

[48] R. P. van der Marel, D. R. Alves, E. Hardy and N. B. Suntzeff, Astron. J. **124** (2002) 2639

[49] P. Gondolo and J. I. Silk, Phys. Rev. Lett. **83** (1999) 1719

[50] D. Merritt, M. Milosavljevic, L. Verde and R. Jimenez, Phys. Rev. Lett. **88** (2002) 191301

High energy γ -ray detectors

	HESS (I)	VERITAS	MAGIC	EGRET	GLAST
Energy	40 GeV-10 TeV	50 GeV-10 TeV	30 GeV-10 TeV	20 MeV-30 GeV	20 MeV-300 GeV
σ_E/E	$\approx 10\%$	$\approx 15\%$	$\approx 20\%$	$< 10\%$	$\approx 5\% > 10$ GeV
A_{eff} (cm 2)	$4 \times 10^8 (> 100 \text{ GeV})$	$4 \times 10^8 (> 100 \text{ GeV})$	$4 \times 10^8 (> 100 \text{ GeV})$	1.5×10^3	10^4
Φ_{min} (cm $^{-2}$ s $^{-1}$)	$8 \times 10^{-12} (> 100 \text{ GeV})$	$9 \times 10^{-12} (> 100 \text{ GeV})$	$\approx 10^{-11} (> 100 \text{ GeV})$	$10^{-7} (> 100 \text{ MeV})$	$310^{-9} (> 100$
Ang. res. (single γ)	$< 0.1^\circ$ at 100 GeV	$< 0.1^\circ$ at 100 GeV	$\approx 0.2^\circ$	$< 5.8^\circ$ at 100 MeV	2° at 100 MeV 0.1° at 10 GeV
Field of view	$4.3^\circ - 5^\circ$	3.5°	$\approx 5^\circ$	0.5 sr	2.4 sr

TABLE IV: Performance of the gamma-ray detectors. Numbers quoted correspond to 5σ sensitivity after 50 hours of observation